Journal of
Intelligent Material
Systems and Structures

Original Article

Journal of Intelligent Material Systems and Structures
2018, Vol. 29(7) 1348–1359

DOI: 10.1177/1045389X17733329
journals.sagepub.com/home/jim
SAGE

Model and experimental research of a hybrid self-contained electro-hydrostatic actuator using piezoelectric stack

Yazi Guo[1], Yuchuan Zhu[1], Yuyang Li[1], Shangshu Fei[1], Bin Zhu[1], Xinbin Zhang[2,3] and Xiaolu Wang[2,3]

Abstract

Smart material–based electro-hydrostatic actuators are a potential alternative to traditional hydraulic actuators. Piezoelectric materials are a type of smart materials that can deliver large blocked forces. In this article, a piezoelectric stack–based electro-hydrostatic actuator is first introduced by presenting the schematic diagrams of its structure and work principle. Next, according to the research of the piezoelectric stack–based electro-hydrostatic actuator working principle, a mathematical model that can describe the dynamic characteristics of piezoelectric stack–based electro-hydrostatic actuator was established. The output displacement model of the piezoelectric stack–based actuator was established based on the improved asymmetric Bouc–Wen model. The simulation model was built in MATLAB/Simulink. Finally, experiments under different working conditions were conducted, as well as the corresponding simulations. The experimental results demonstrate that the prototype no-load output flow reaches its maximum at 275 Hz and the output flow peak is close to 1.6 L/min. Moreover, the load capacity is more than 20 kg and the maximum load is more than 50 kg according to the trend forecast. The simulation results exhibit good agreement with the experimental results, which means that the piezoelectric stack–based electro-hydrostatic actuator model is feasible.

Keywords

Piezoelectric stack, electro-hydrostatic actuator, mathematical model, Bouc–Wen model, output flow

Introduction

Conventional hydraulic actuators are potential choices for applications in aerospace because they can offer reliable performance with high forces and large displacement capabilities. However, typical hydraulic actuators rely heavily on a distributed pipeline heavily. This is one of the main disadvantages of using conventional hydraulic actuators which limits the application of the conventional hydraulic systems in some fields, such as unmanned aerial vehicles and rotorcraft.

Intelligent materials and intelligent material–based actuators have an increasing range of applications both in aerospace and in civil engineering (Zhu et al., 2016; Zhu and Ji, 2014; Zhu and Li, 2014, 2015), As a solution, an intelligent material–based electro-hydrostatic actuator can be one of the potential alternatives that can replace the conventional hydraulic actuator system in the modern aerospace field (Li et al., 2004).

A hybrid hydraulic actuator driven by various intelligent materials, which can eliminate the distributed pipeline, has recently become a valuable research area. Integrated, stable, and high-bandwidth actuator systems have become a necessity for modern airborne hydraulic systems in the era of power-by-wire. Along with the development of intelligent material technology, the electro-hydrostatic actuator based on intelligent material is becoming an important direction for the new generation of airborne actuators (Sha and Li, 2004).

[1]College of Mechanical and Electrical Engineering, Nanjing University of Aeronautics and Astronautics, Nanjing, China
[2]Shanghai Aerospace Control Technology Institute, Shanghai, China
[3]Shanghai Engineering Research Center of Servo Systems, Shanghai, China

Corresponding author:
Yuchuan Zhu, College of Mechanical and Electrical Engineering, Nanjing University of Aeronautics and Astronautics, Box 347, No. 29 Yudao Street, Nanjing 210016, Jiangsu, China.
Email: meeyczhu@nuaa.edu.cn

Piezoelectric material, an example of intelligent materials, is known for its large rigidity, high energy density, and broad frequency bandwidth. Recently, the piezoelectric material–based actuator driven by a piezoelectric stack has been studied widely both locally and globally. The technology of piezoelectric stack–based electro-hydrostatic actuator (PEHA) aims to create systems that allow the application of mechanical power output through hydraulics without a distributed pipeline of a conventional hydraulic system. The basic operation of the piezoelectric actuator driven by a piezoelectric stack involves high-frequency bidirectional operation of the piezoelectric stack, which is converted to unidirectional motion of the transmission fluid by flow rectification using a set of passive valves. As a result, the complexity of the fluid transmission is reduced using the piezoelectric stack to drive the fluid directly, and thus, the distributed pipelines can be eliminated (Sanders et al., 2004; Tao, 1997). However, the inherent hysteresis and nonlinearities in piezoelectric material are the major barriers for establishing a mathematic model. Moreover, the piezoelectric material hysteresis is apparently rate dependent. Generally, the dynamic hysteresis is of less interest while investigating the performance of actuators, and it is more important to model the actual hysteretic behaviors of the actuator. Many hysteresis models have been used to do this work (Chopra and Sirohi, 2013).

Thomas Hegewald et al. (2008) proposed a method based on the Jiles-Atherton model to model the hysteresis of the piezoelectric stack–based actuator (PSA) based on the Jiles–Atherton model. The method used the concept of electric polarization of the piezoelectric material and defined a hysteresis operator involved with an irreversible part and a reversible part of the polarization. This model provided deep insight into the physical processes of the polarization and tracked the hysteresis well; however, the method seems to fail to describe the dynamic characteristic. The Preisach model and its simplified Prandtl–Ishlinskii (PI) model are widely used for modeling piezoelectric material. Sreeram and Naganathan (1994) used the Preisach model to model the hysteresis of the PSA. Dong and Tan (2009) conducted research on the application of the PI model used in the process of modeling PSA. However, these models are symmetric or static models and can be improved. Bouc–Wen model (Ismail et al., 2009) is a first-order differential equation of simple form and easy to implement. Since traditional Bouc–Wen model cannot track the asymmetric characteristic of the piezoelectric material hysteresis, corresponding improved models have been proposed. Related research (Li et al., 2013; Song and Kiureghian, 2006) used improved forms of the traditional Bouc–Wen model and make the model capable of describing the asymmetric characteristics. Zhu Wei and Rui (2016) proposed a method to establish the dynamic model of the PSA using an asymmetric Bouc–Wen model and succeed to track the PSA output displacement within 100 Hz.

PSA is the core component of PEHA. In the early stage of the study in this field, a PEHA developed by Konishi (1999) can produce 18 W output power and reach its maximum output flow at approximately 300 Hz. The piezoelectric stack used here is 55.5 mm long and its diameter is 22 mm. A piezo-hydraulic actuator was constructed by Tang et al. (1995), and this research aimed to solve the active vibration control problem of rotor dynamic systems. Piezoelectric materials possess the ability to deliver the large force and operate at high frequency. A piezoelectric stack–based device developed by Mauck and Lynch (2000) had a power output of approximately 18 W and a blocked force of 271.7 N. However, its working frequency was less than 100 Hz which is relatively low and used passive valves to perform frequency rectification. Sirohi and Chopra (2002) developed a compact hybrid hydraulic actuator that could be driven by magnetostrictive and piezoelectric stacks. Using piezoelectric stacks, this actuator had an output power of 2.5 W, blocked force of approximately 138 N and operated at relatively higher pumping frequency. Ullmann and Fono (2002) developed a valveless piezoelectric pump that used appropriately shaped and directed nozzles to rectify the flow. Kim and Wang (2010a) conducted a study of design and nonlinear force control of a power-by-wire piezoelectric hydraulic pump actuator for automotive transmissions.

This article aims to research the output flow of the PEHA and verify the practicability of the PEHA model. Then, the best output performance of the prototype will be found, and in order to provide some guidelines for the design of the PEHA. First, the structure configuration of the PEHA prototype is proposed and the working principle of the actuator is analyzed. Second, the overall dynamic mathematical model of the system is established. Finally, the simulation and experiment output flow of the prototype is got respectively and the practicability of the model is verified by comparing experimental output flow with model output flow. To verify the stability of the prototype output performance, the experiments were carried out under a no-load condition and a loaded condition, and corresponding simulations were conducted and compared.

Based on the PEHA work principle, a dynamic model of the piezoelectric-based actuator based on the improved asymmetric Bouc–Wen model was first established first. The pump chamber model of the PEHA, the simplified reed valve model, the fluid model of the fluid flowing in the tube, and the PEHA hydraulic cylinder model were incorporated into the whole system model.

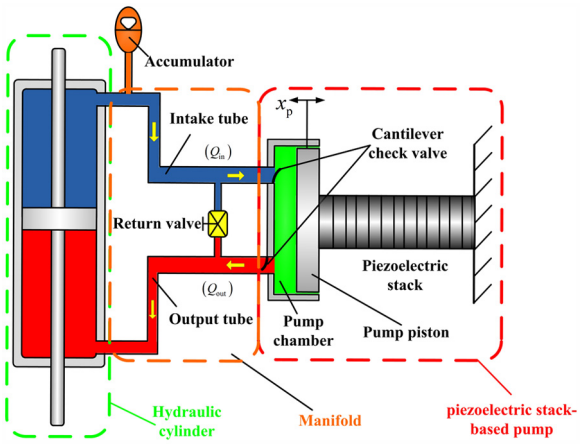

Figure 1. Operation principle of PEHA.

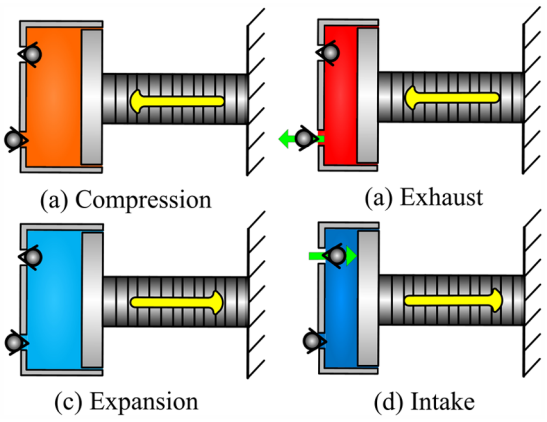

Figure 2. Operation stages of PSP.

Configuration and working principle of the PEHA

Structure configuration

First, a PEHA is shown by presenting its structure configuration. PEHA's primary structure is composed of four parts: a piezoelectric stack–based pump (PSP), a fluid transmission and control section (manifold), a hydraulic cylinder, and an accumulator.

The PEHA utilizes fluid rectification via two one-way check valves to amplify the small, high-frequency vibrations of the piezoelectric stack into large motions of the hydraulic cylinder. An accumulator is connected to the low-pressure side of the PEHA by a connecting tube.

Working principle

As shown in Figure 1, the PSP provides energy for the system as the driving element. The periodic input voltage applied on the piezoelectric stack can form an electric field that induces polarization in the piezoelectric material and drives the piezoelectric stack to produce displacement. Therefore, the pump cavity piston will move back and forth constantly. Then, the pump chamber will absorb and drain fluid due to the change in the volume. The micro flow will contribute to the output of the hydraulic cylinder using the principle of frequency rectification which is performed by passive unidirectional reed valves.

As shown in Figure 2, the operation of the PSP can be divided into four distinct stages as follows (Chaudhuri and Wereley, 2010, 2012):

1. *Compression*. With sinusoidal electricity supply, expansion of the piezoelectric stack pushes hydraulic fluid into the closed pump chamber, resulting in the increase of pressure in the chamber.
2. *Exhaust*. The outlet valve was opened due to the pressure difference between both side of outlet valve, so fluid starts to flow out of the chamber into the outlet tube, and the pressure builds up in the high-pressure-driven side of the output cylinder and resulting in motion of the output shaft.
3. *Expansion*. The piezoelectric stack starts to retreat with decreasing applied field, causing a pressure drop in pump chamber.
4. *Intake*. The pressure in the pump chamber drops further to open the intake reed valve and allows fluid to flow from the low-pressure-driven side of the output cylinder back into the chamber.

These four stages are repeated every pump cycle and result in a fluid flow out of the pump through the discharge tube and back into the pump through the intake tube. Through this stepwise actuation process, the high frequency, small stroke of the piezoelectric stack is converted into a larger displacement of the output cylinder.

PEHA mathematical model

Based on the above analysis, the mathematical model of PEHA will be established in this section. The system model consists of the driving model, the pump chamber model, the reed valve model, the fluid tubing model, and the cylinder output model.

PEHA driving model

PSA is the driving element of the PEHA and the mathematical model of the PSA should be established first.

PSA static model based on Bouc–Wen model. The PSA output displacement exhibits nonlinear characteristics of frequency-dependent hysteresis. First, a static model was established using the asymmetric Bouc–Wen

model. This hysteresis model is an improvement on the classical Bouc–Wen model which aims to describe asymmetric hysteresis systems. The PSA output displacement model based on the asymmetric Bouc–Wen model can be described as follows (Low and Guo, 1995)

$$\begin{cases} x = a \cdot u - h \\ \dot{h} = \dot{u}[\alpha - |h|\varphi(\dot{u}, h)] \\ \varphi(\dot{u}, h) = \varphi_1 \operatorname{sgn}(\dot{u}h) + \varphi_2 \operatorname{sgn}(\dot{u}) + \varphi_3 \operatorname{sgn}(h) + \gamma \end{cases} \tag{1}$$

where x is the output displacement, u is the driving voltage, a is a scaling factor between the output displacement and the input voltage, h is a lag portion of the output displacement, and $d \cdot u$ represents the linear portion of the output displacement.

PSA dynamic model. Obviously, the hysteresis of the PSA output displacement is rate dependent. Therefore, a dynamic model of the PSA is established based on the system kinetic equations. The output force was divided into a linear portion and a lag portion according to the analysis method of the output displacement. A lag segment was established between the input voltage and linear force. The response time was identified according to the PSA step response experiment (Wang et al., 2015; Zhu and Rui, 2016). The dynamic model of the PSA can be described as follows

$$\begin{gathered} m_0\ddot{x} + c_0\dot{x} + k_0(x - x_{\text{ini}}) = F_0 = \frac{k_{\text{u}}}{\tau} e^{-\frac{t}{\tau}} u + kh \\ \dot{h} = \dot{u}[\alpha - |h|\varphi(\dot{u}, h)] \\ \varphi(\dot{u}, h) = \varphi_1 \operatorname{sgn}(\dot{u}h) + \varphi_2 \operatorname{sgn}(\dot{u}) + \varphi_3 \operatorname{sgn}(h) + \gamma \end{gathered} \tag{2}$$

where m_0, c_0, k_0 are the equivalent mass, stiffness, and damping of the piezoelectric stack, respectively. τ is the time constant and k_{u} is the scale factor between the linear output force and the input voltage.

PEHA driving model. As part of the whole system, the driving model of the PEHA can be described in the following while the PSA is working with other components. As shown in Figure 3, the driving part of the PEHA is considered as a single-degree-of-freedom system. The motion equation of the piston is proposed as follows (John et al., 2008)

$$\begin{gathered} (m_0 + m_{\text{p}} + m_{\text{r}})\ddot{x}_{\text{p}} + (c_0 + c_{\text{r}})\dot{x}_{\text{p}} + (k_0 + k_{\text{B}} + k_{\text{d}}) \\ x_{\text{p}} = F_0 - p_{\text{c}}A_{\text{p}} \end{gathered} \tag{3}$$

where m_{p}, m_{r} are the mass of the piston and the output rod, respectively; c_{r} is the damping constant of pump piston; k_{d}, k_{B} is the stiffness of the metal diaphragm disk spring; p_{c} is the pressure of pump chamber; and A_{p} is cross-sectional area of piston.

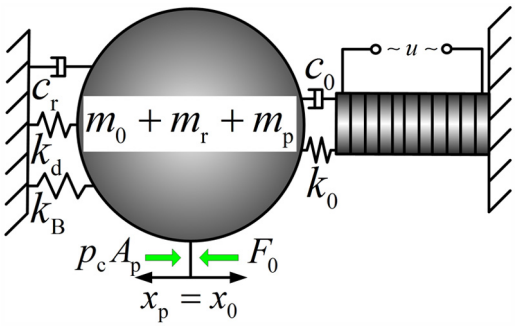

Figure 3. Kinetic model of PEHA driving part.

PEHA pump chamber model

According to the compression stage, the fluid in the pump chamber is compressed to flow out of the chamber. The fluid bulk modulus is a key parameter to describe the fluid compression, which can be defined as (Chaudhuri, 2008; Kim and Wang, 2010)

$$\beta = -\frac{\Delta p}{\Delta V} V \Rightarrow dP = -\beta \frac{\mathrm{d}V}{V} \Rightarrow \dot{P} = -\beta \frac{\dot{V}}{V} \tag{4}$$

where β represents the bulk modulus of the fluid, V is the volume of the fluid, and ΔV is the change of the fluid volume based on the pressure increase Δp.

The pure oil can be considered as incompressible. However, the bulk modulus will decline dramatically because of the entrapped air. Therefore, the effective bulk modulus can be defined as (Kim and Wang, 2009b)

$$\frac{1}{\beta_{\text{e}}} = \lambda_{\text{a}} \cdot \frac{p_{\text{a}}}{p_{\text{f}}^2} + \left(1 - \lambda_{\text{a}} \cdot \frac{p_{\text{a}}}{p_{\text{f}}}\right) \frac{1}{\beta_{\text{f}}} \tag{5}$$

where β_{e} represents the effective bulk modulus, p_{a} is atmospheric pressure, p_{f} is the applying pressure on the fluid, and λ_{a} is the entrapped air volume fraction and can be defined as

$$\lambda_{\text{a}} = \frac{V_{\text{a}}}{V_{\text{a}} + V_{\text{o}}} \tag{6}$$

where V_{a}, V_{o} are the volume of entrained air and the oil, respectively. It is clear that the increase in the applying pressure can improve the effective bulk modulus.

As we know

$$m = \rho \cdot V \Rightarrow \frac{\dot{\rho}}{\rho} = \frac{\dot{m}/\rho - \dot{V}}{V} \tag{7}$$

As shown in Figure 4, the fluid flow in the pump chamber can be described as (Kim and Wang, 2009)

$$\frac{\dot{\rho}_{\text{c}}}{\rho_{\text{c}}} = \frac{(Q_{\text{in}} - Q_{\text{out}} - Q_{\text{le}}) - A_{\text{p}}\dot{x}_{\text{p}}}{A_{\text{p}}(h - x_{\text{p}})} \tag{8}$$

For an enclosed volume, the fluid mass remains unchanged and formulation (7) can be simplified as

$$\frac{\dot{\rho}}{\rho} = -\frac{\dot{V}}{V} \tag{9}$$

According to formulations (4) and (9), we can get

$$\dot{P} = \beta\frac{\dot{\rho}}{\rho} \tag{10}$$

Based on formulations (8) and (10), the model of the pump chamber can be defined as follows (Chaudhuri, 2008; Chaudhuri et al., 2009)

$$\dot{p}_c = \beta_e \frac{A_p\dot{x}_p + Q_{out} - Q_{in} - Q_{le}}{A_p(h - x_p)} \tag{11}$$

where Q_{in}, Q_{out}, Q_{le}, and h are the intake flow, the outlet flow, the leakage flow, and the height of pump chamber, respectively.

PEHA valve model

The actual working conditions of the cantilever reed valves in the PEHA are rather complicated because of the fluid–structure interaction problem. To simplify the problem, a single-degree-of-freedom system is used here to model the valves (Kim and Wang, 2009; Walters, 2008).

In general, a single-degree-of-freedom model can be defined as follows

$$m\ddot{x} + c\dot{x} + kx = F \tag{12}$$

As shown in Figure 5, m, c, k, and F are the system mass, damp, stiffness, and force, respectively. In the process of the reed valve modeling, the mass, damp, and stiffness of the reed valve are replaced by the reed valve plate equivalent value: m_R, c_R, k_R. P_1, P_2 represent the pressures on the two sides of the reed valve, corresponding to the P_c, P_{th} and P_{tl}, P_c in the process of discharge oil and intake oil. Therefore, the opening displacement of the inlet valve (x_{Ri}) and outlet valve (x_{Ro}) can be expressed as follows

$$\begin{cases} m_R\ddot{x}_{Ri} + c_R\dot{x}_{Ri} + k_Rx_{Ri} = A_R(p_{tl} - p_c) \\ m_R\ddot{x}_{Ro} + c_R\dot{x}_{Ro} + k_Rx_{Ro} = A_R(p_c - p_{th}) \end{cases} \tag{13}$$

where A_R is the effective area of the reed valve.

The general form of the orifice equation can be written as

$$Q = \begin{cases} c_vA_o\sqrt{\frac{2|\Delta p|}{\rho}} & \Delta p = p_1 - p_2 > 0 \\ -c_vA_o\sqrt{\frac{2|\Delta p|}{\rho}} & \Delta p = p_1 - p_2 < 0 \end{cases} \tag{14}$$

where c_v is the discharging flow coefficient of the valve port, and A_o is the orifice area. Therefore, the flow

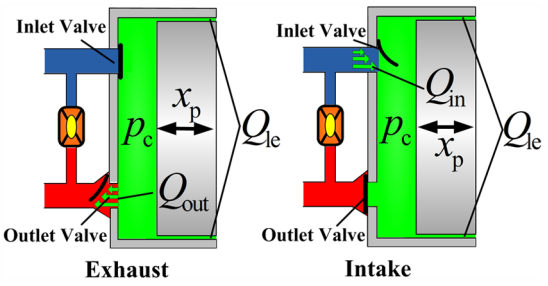

Figure 4. Working process of the pump chamber.

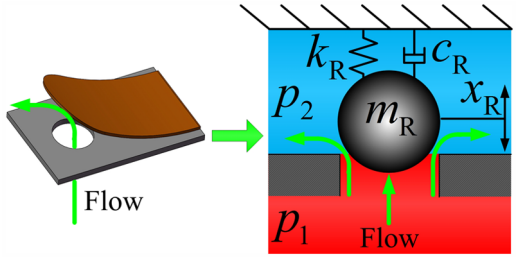

Figure 5. A single-degree-of-freedom model for reed valve.

through the valve can be written as (Chaudhuri A 2008, Kim GW 2009, Walters TE 2008)

$$\begin{cases} Q_{in} = \mathrm{sgn}(p_{tl} - p_c)c_dwx_{Ri}\sqrt{\frac{2}{\rho}|p_{tl} - p_c|}, \\ x_{Ri} = \begin{cases} x_{Ri}, x_{Ri} > 0 \\ 0, x_{Ri} \le 0 \end{cases} \\ Q_{out} = \mathrm{sgn}(p_c - p_{th})c_dwx_{Ro}\sqrt{\frac{2}{\rho}|p_c - p_{th}|}, \\ x_{Ro} = \begin{cases} x_{Ro}, x_{Ro} > 0 \\ 0, x_{Ro} \le 0 \end{cases} \end{cases} \tag{15}$$

where w is the orifice area gradient.

PEHA fluid model

The fluid model is shown in Figure 6.

As shown in Figure 6, at the exhaust stage, the fluids flow out of the chamber into the discharge tube and accumulate in the hydraulic cylinder. Therefore, the pressure of the high-pressure-driven side of the hydraulic cylinder increases and pushes the hydraulic cylinder piston. The working process in the low-pressure side of the hydraulic cylinder is similar, causing the fluid will flow back to the pump chamber.

The definition of the Reynolds number can be defined as

$$R_e = \frac{\rho v d}{\mu} \tag{16}$$

where ρ is the oil density, v is the fluid velocity, μ is the oil dynamic viscosity, and d is the diameter of the tube.

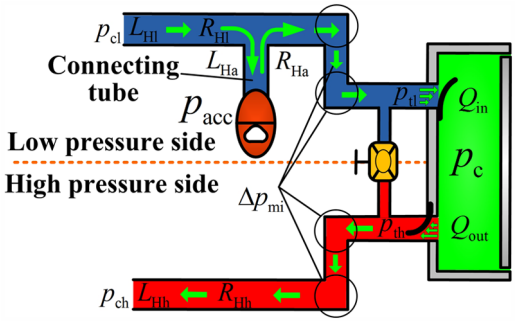

Figure 6. Illustration of the fluid in the tube.

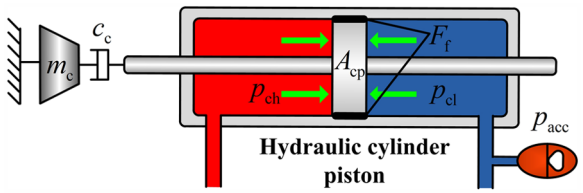

Figure 7. Schematic of fluid flow in hydraulic cylinder.

According to the definition, the flow state can be simplified as incompressible laminar flow in the tube.

From the perspective of energy conservation, the kinetic energy of the fluid suffers losses for the following reasons: the fluid resistance because of the presence of oil viscosity, inertial force because of the velocity variation, minor loss, and the influence of the fluid capacitance. Considering the above factors comprehensively, and the model for the fluid flowing in the high-pressure side tube can be derived as (Chaudhuri and Wereley, 2012; Kim and Wang, 2009)

$$p_{th} - p_{ch} = \dot{Q}_{out} L_{Hh} + Q_{out} R_{Hh} + \Delta p_{mih} \tag{17}$$

$$\dot{p}_{ch} = \beta_{ech} \frac{Q_{out} - \dot{x}_{cp} A_{cp}}{(x_{0cp} + x_{cp}) A_{cp}} \tag{18}$$

where p_{ch} is the pressure at the interface of the high-pressure side tubing and the hydraulic cylinder; p_{th} is the pressure at the interface of the high-pressure side tubing and the pump chamber; L_{Hh}, R_{Hh} are the fluid resistance and inductance in the high-pressure side tubing; β_{ech} is the effective bulk modulus of the high-pressure side of the hydraulic cylinder; x_{cp} is the displacement of the hydraulic cylinder output rod; A_{cp} is the effective area of the cylinder piston; and x_{0cp} is the initial position of the cylinder rod.

The fluid resistance L_H can be calculated according to the following formula

$$L_H = \frac{\rho l_t}{A_t} \tag{19}$$

where l_t, A_t are the length and cross-sectional area of the high-pressure side tube, respectively.

According to the Hagen–Poiseuille equation, the fluid resistance can be derived as follows

$$\Delta p_{vis} = \frac{128\mu}{\pi D^4} lQ \Rightarrow R_{ht} = \frac{8\pi\mu l_{ht}}{A_t^2} \tag{20}$$

where Δp_{vis} represents the viscosity loss because of the viscous fluid.

The minor loss of the fluid flowing through the entrance and corner can be expressed as follows

$$\Delta P_{mi} = \frac{\rho}{2} \sum_{i=1}^{n=3} \left(\xi_i \frac{Q_{out}^2}{A_t^2} \right) \tag{21}$$

where ξ_i is the minor loss coefficient which can be referenced (Chaudhuri, 2008).

In general, the working process of the fluid flowing in the low-pressure side tube from the cylinder to the accumulator port and the working process of the fluid flowing in the low-pressure side tube from the accumulator to the inlet valve port are similar. The model expressions of the three processes are the same.

PEHA hydraulic cylinder model

According to the analysis above, the pressure on the two sides of the piston is not equal and acts as the power source of the hydraulic cylinder output rod motion.

Additionally, the motion of the output rod is influenced by such factors as viscous and friction force and gravity. Therefore, based on Newton's laws of motion and kinetic equations in general, the PEHA hydraulic cylinder model can be simply defined as (Kim and Wang, 2010; Tan et al., 2010; Walters, 2008)

$$m_c \ddot{x}_{cp} + c_c \dot{x}_{cp} = (p_{ch} - p_{cl}) A_{cp} - F_f - m_c g \tag{22}$$

As shown in Figure 7, m_c represents the mass of the load (including the output rod), c_c is the movement damping, and F_f is the total motion friction.

Parameters identification method and experimental system configuration

PSA dynamic model parameters identification

To identify the parameters of the PSA dynamic model, two special working conditions are selected here to simplify the identification process. And the model is divided into a linear part and a nonlinear part.

Identification method of the linear part parameters. The PSA can be simplified to a linear system while the driving voltage amplitude is less than its rated working voltage (Zhu and Rui, 2016; Zhu and Wang, 2012). And this means that the hysteresis part of the output

displacement can be ignored. Therefore, the PSA model can be written as

$$m\ddot{x}_s + c\dot{x}_s + k(x_s - x_0) = \frac{k_u}{\tau}e^{-\frac{t}{\tau}}u \tag{23}$$

$$\dot{h} = \dot{u}[\alpha - |h|\varphi(\dot{u}, h)] \tag{24}$$

$$\varphi(\dot{u}, h) = \varphi_1 \operatorname{sgn}(\dot{u}h) + \varphi_2 \operatorname{sgn}(\dot{u}) + \varphi_3 \operatorname{sgn}(h) + \gamma \tag{25}$$

Under zero initial conditions, the transfer function of the simplified model according to the Laplace transform can be written as

$$\frac{x(s)}{u(s)} = G(s) = \frac{k_u\tau}{\tau s + 1} \cdot \frac{1}{ms^2 + cs + k} \tag{26}$$

where m, c, and k are the mass, damping, and stiffness of the piezoelectric stack, respectively, and can be obtained according to the performance test results performed by the product vendor. Therefore, the time constant τ can be obtained by a step response experiment of the PSA. Finally, the coefficient k_u can also be obtained by a step response experiment of the PSA.

Identification method of the nonlinear part parameters. Likewise, the PSA can be simplified to a quasi-static system when the driving voltage frequency is low enough. This means that the impact of the output displacement variation and the time constant τ is small. Thus, the velocity term and the acceleration term can be ignored. Meanwhile, $(1/\tau)e^{-t/\tau} \approx 1$ (Zhu and Rui, 2016; Zhu and Wang, 2012). Therefore, the PSA model can be written as

$$kx = k_u u + kh \tag{27}$$

$$\begin{cases} \dot{h} = \dot{u}[\alpha - |h|\varphi(\dot{u}, h)] \\ \varphi(\dot{u}, h) = \varphi_1 \operatorname{sgn}(\dot{u}h) + \varphi_2 \operatorname{sgn}(\dot{u}) + \varphi_3 \operatorname{sgn}(h) + \gamma \end{cases} \tag{28}$$

According to formulation (27), we obtain

$$k\dot{x} = k_u\dot{u} + k\dot{h} \tag{29}$$

The driving voltage is limited to be small enough so that we can ignore the hysteresis part of the output displacement and formulation (28) can be written as

$$\dot{h} = \dot{u} \cdot \alpha \tag{30}$$

Assuming that (u_i, x_i) is the solution of equation (29) in the ith ($i = 1, 2, \ldots, N_1$) experimental period and according to formulations (29) and (30), we obtain

$$\alpha_i = \frac{k\dot{x}_i - k_u\dot{u}_i}{k\dot{u}_i} \tag{31}$$

Therefore, we can get

$$\alpha = \frac{1}{N}\sum_{i=1}^{N}\frac{k\dot{x}_i - k_u\dot{u}_i}{k\dot{u}_i} \tag{32}$$

And in the four different areas, formulation (28) can be expressed as

$$\dot{u}(t) > 0 \text{ and } h > 0,\ \dot{h} = \dot{u}\alpha - \dot{u}h(\varphi_1 + \varphi_2 + \varphi_3 + \gamma)$$
$$\dot{u}(t) > 0 \text{ and } h < 0,\ \dot{h} = \dot{u}\alpha + \dot{u}h(-\varphi_1 + \varphi_2 - \varphi_3 + \gamma)$$
$$\dot{u}(t) < 0 \text{ and } h > 0,\ \dot{h} = \dot{u}\alpha - \dot{u}h(-\varphi_1 - \varphi_2 + \varphi_3 + \gamma)$$
$$\dot{u}(t) < 0 \text{ and } h < 0,\ \dot{h} = \dot{u}\alpha + \dot{u}h(\varphi_1 - \varphi_2 - \varphi_3 + \gamma)$$

Therefore, four independent experimental data are enough for solving simultaneous equations to identify the parameters φ_1, φ_2, φ_3, and γ. Generally, in the four different areas, each set of $u_1 \ldots u_i \ldots u_N$ and corresponding $h_1 \ldots h_i \ldots h_N$ can obtain a set of solutions. An optimal solution can be obtained according to the principle of least squares. In summary, with the experimental data collected by the laser displacement sensor and force sensor under certain driving conditions, it is possible to identify the above parameters.

Simulation model configuration and parameters

The PEHA simulation model is shown in Figure 8.

Based on the analysis above, the simulation model of the PEHA is established in MATLAB/Simulink. The major parameters of the PEHA simulation model are listed in Table 1.

Test bench configuration

As shown in Figure 9, a signal generator was used to provide a sinusoidal bias voltage signal, which was amplified by the power amplifier and drive the piezoelectric stack. An eddy current displacement was used to measure the PSA output displacement. The displacement data and the output signal of the power amplifier were stored by the oscilloscope at the same time. A laser displacement sensor was used here to measure the PEHA hydraulic cylinder output displacement. A force sensor is installed in the bottom of the PSA, the output signal of the power amplifier and the force data were also stored by the oscilloscope at the same time.

The accumulator plays an important role in the system. It can provide a bias pressure to prevent cavitation, improve the stiffness of fluid, compensate for leakage of fluid, and assist in applying a pre-stress on the piezoelectric stack. During the PEHA experiment, the accumulator was closed after compensating for leakage to exclude its influence.

According to the model above, the parameters were identified through experiments and mathematical derivation, and the dynamic model of PSA and PEHA was

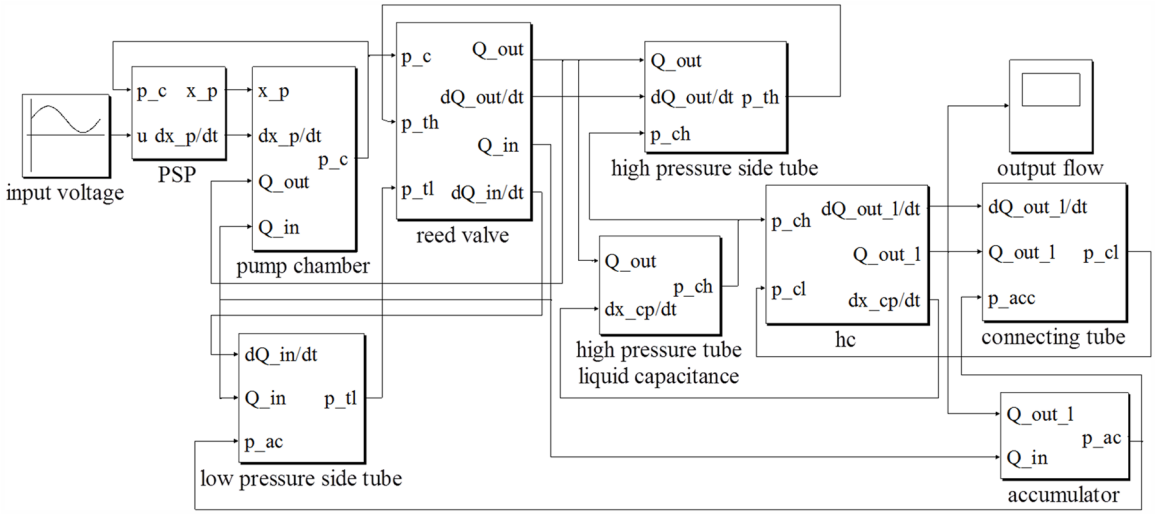

Figure 8. MATLAB/Simulink simulation model for PEHA.

Table 1. PEHA simulation parameters.

Name	Unit	Symbol	Value
Piezoelectric stack mass	kg	m_0	0.062
Piezoelectric stack damp	N s m^{-1}	c_0	2000
Piezoelectric stack stiffness	N/m	k_0	70e6
Time constant	S	τ	5e–5
B-W model parameters1	μm/V	a	0.57
B-W model parameters2	μm/V	α	0.2392
B-W model parameters3	V^{-1}	γ	−0.0839
B-W model parameters4	V^{-1}	φ_1	0.1109
B-W model parameters5	V^{-1}	φ_2	−0.1075
B-W model parameters6	V^{-1}	φ_3	0.0803
Pump piston mass	kg	m_p	0.012
Pump chamber height	mm	h	0.5
Pump chamber radius	mm	r_c	23
Pure oil bulk modulus	MPa	β_f	1800
Orifice area gradient	1	w	3.14×10^{-3}
Fluid density	kg/m^3	ρ	875
Reed valve thickness	mm	h_R	0.15
Entrained air fraction	–	λ_a	5%
Tube diameter	mm	D_t	4
Reed valve equivalent mass	kg	m_R	1e–3
Reed valve stiffness	N/m	k_R	13500
Reed valve damp	N s m^{-1}	c_R	7
Reed valve area	m^2	A_R	1.256e–5
Orifice flow coefficient	–	c_v	0.7

built in MATLAB/Simulink. Experimental and simulation results are shown in the following.

Simulation and experimental verification

PSA output displacement experiment

Based on the preparation above, the PSA output displacement experiment and simulation were performed, and the results are shown in Figure 10.

Considering that the piezoelectric stack cannot withstand reverse voltage, a sinusoidal voltage signal with DC bias was chosen as the driving signal. The driving signal generated by amplifier was 100 Vpp, 50 DC (Direct-current). The driving signal generated by amplifier was 100 Vpp, 50 DC. The experiment data were collected by using different frequency sinusoidal voltage. The results are shown in the following.

PEHA output performance experiment

Output flow is a comprehensive indicator of the cylinder output force and speed. Therefore, it is used as a

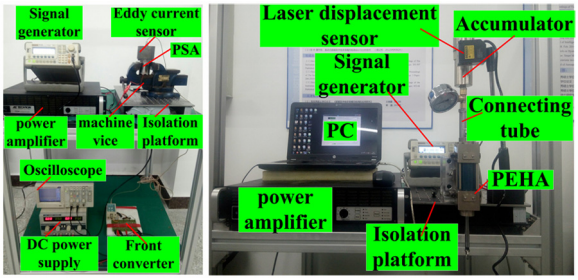

Figure 9. Experimental test bench.

major indicator to measure the output performance of the PEHA. The PEHA no-load performance and load performance were tested under different conditions. Because the piezoelectric stack used in this research cannot withstand reverse voltage, the input voltages in the following experiments were all sinusoidal signals with DC bias. The rated voltage of the piezoelectric stack used here cannot exceed 150 V. To achieve a higher output flow and protect the piezoelectric stack as well, the magnitude of the driving voltage did not exceed 140 Vpp. Meanwhile, the working frequency was limited to 450 Hz while the input voltage was 140 Vpp with 70 VDC due to the power limitation of the power amplifier.

The PEHA output flow was inferred by measuring the cylinder shaft displacement, and the trend of the output flow with increasing frequency under different accumulator bias pressures is shown in Figure 9. The tests were conducted under 0.6 MPa bias pressure and 1.0 MPa bias pressure, respectively. Input voltage is 140 Vpp with 70 VDC. The results are shown in the following.

As shown in Figure 11, under no-load condition, the prototype output flow reached the maximum at 275 Hz within the 450 Hz range with different driving voltages and bias pressures. While the input voltage was 140 Vpp and the bias pressure was 1.0 MPa, the prototype maximum output flow was close to 1.6 L/min. From the comparison of the two pictures, it is clear that the enhancement of the bias pressure can promote the output flow. According to the effective bulk modulus definition, increasing the bias pressure will reduce the volume fraction of the entrained air in oil and reduce the compressibility of the oil. Therefore, the energy consumed in oil compression will be reduced and the energy transfer efficiency will be improved. This is confirmed by both the experiment and simulation results.

Furthermore, the output flow begins to decline when the frequency exceeds 275 Hz because of the following potential restricting factors: (1) the fluid–structure coupling effect may severely limit the response speed of reed valves, therefore, exacerbating pump backflow at high working frequency, (2) the inertial force has a significant effect on the flow condition and decreases the output flow at high working frequency, and (3) the impact of the fluid resistance and the PSA output displacement hysteresis and other factors become constraints of great significance. More importantly, under different input voltages and bias pressures, the PEHA model simulation results can reflect the prototype

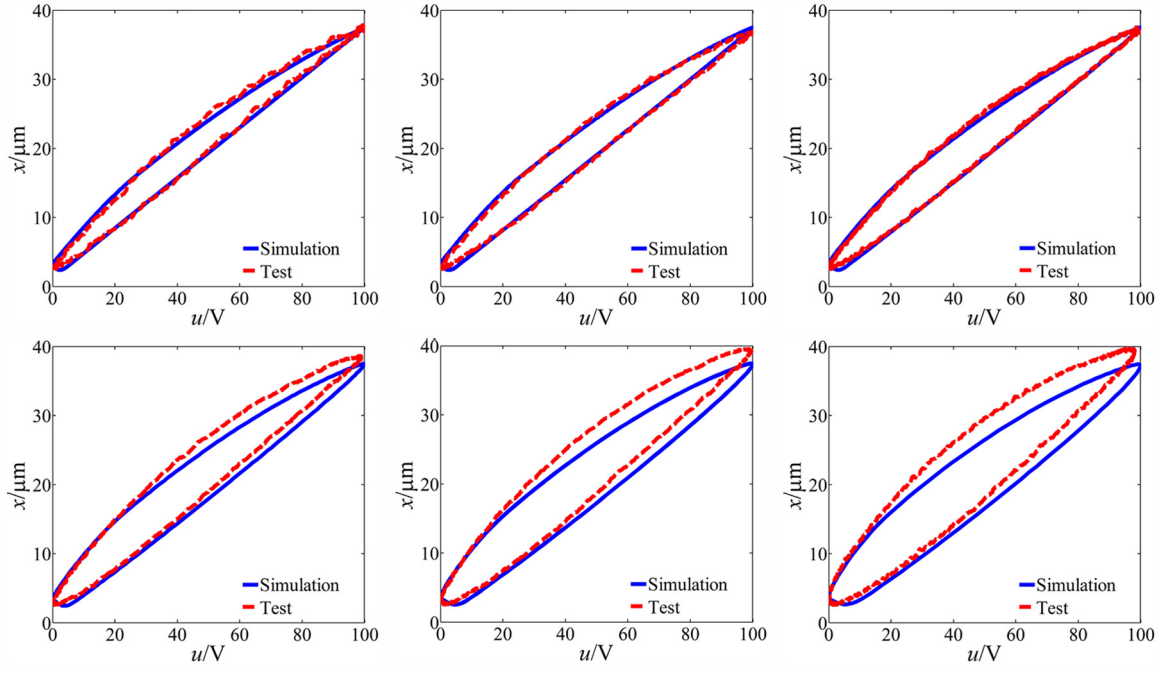

Figure 10. PSA output displacement experiment and simulation.

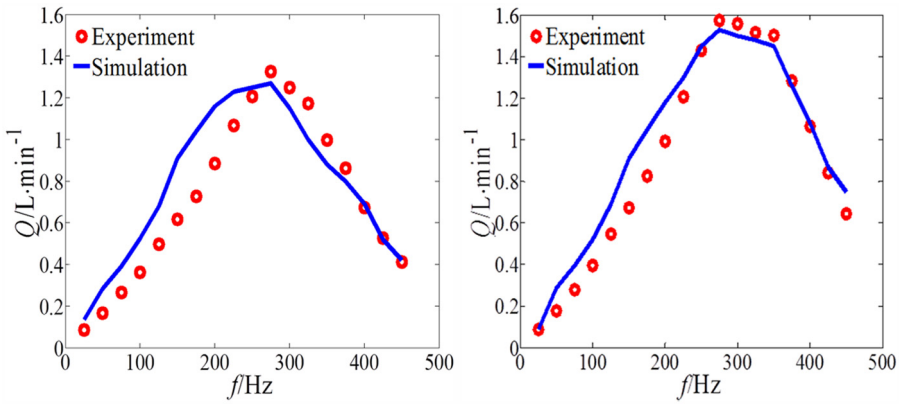

Figure 11. No-load output flow of different bias pressures.

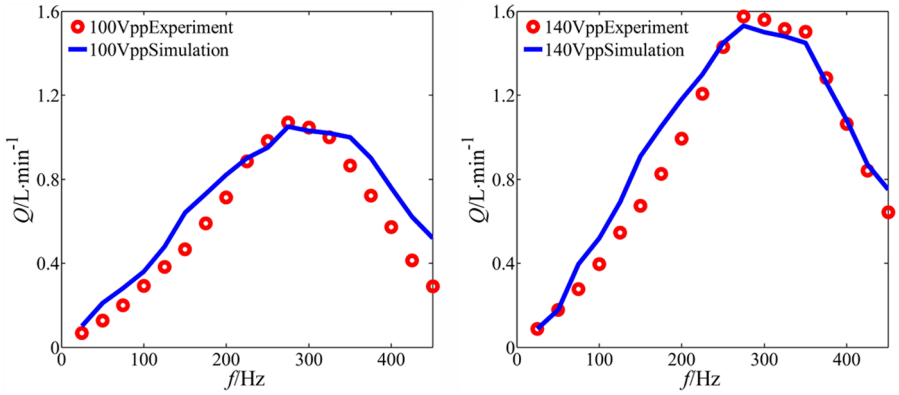

Figure 12. No-load output flow of different voltage magnitudes.

output flow change trend well with error within acceptable limits.

As the driving element of the system, it can be assumed that a larger piezoelectric stack strain will lead to a larger output flow. The magnitude of piezoelectric stack strain is positively correlated with the driving voltage. Therefore, the prototype was tested under 1.0 MPa bias pressure with different input voltages, 100 Vpp with 50 VDC and 140 Vpp with 70 VDC. The experiment and simulation results are shown in Figure 12.

As shown in Figure 12, a larger magnitude of the input voltage corresponds to a larger output flow. The PEHA model simulation results still match the experimental results well under different voltage magnitudes.

As an execution device, PEHA load capacity is an important performance index. To research the prototype load capability, the PEHA output performance was tested by increasing weights attached to the bottom of cylinder output shaft. The experiments were conducted under 1.0 MPa bias pressure with 140 Vpp input voltage. The results are shown in the following:

As shown in Figure 13, the PEHA prototype output flow was reduced as the weight increases, and output flow still achieved nearly 1.0 L/min while driving 20 kg weight, which indicates that the prototype has a fairly good load capacity. Furthermore, the simulation results match the experiment results well while the prototype driving weight.

According to the experiment and simulation results, while the operating frequency was in the vicinity of 275 Hz, the prototype output flow was relatively high. 225, 275, and 325 Hz were chosen to research the output flow change trend. The experiments were conducted under 1.0 MPa bias pressure with 140 Vpp input voltage. The results are shown in the following.

As shown in Figure 14, for a specific working frequencies, the output flow drops steadily as the load increases, and the maximum load capacity is apparently far more than 20 kg at certain frequencies, which shows that the prototype has a relatively good load capacity. The model still predicts the trend of the output flow well.

Conclusion

1. The prototype maximum no-load output flow is close to 1.6 L/min at the peak frequency of

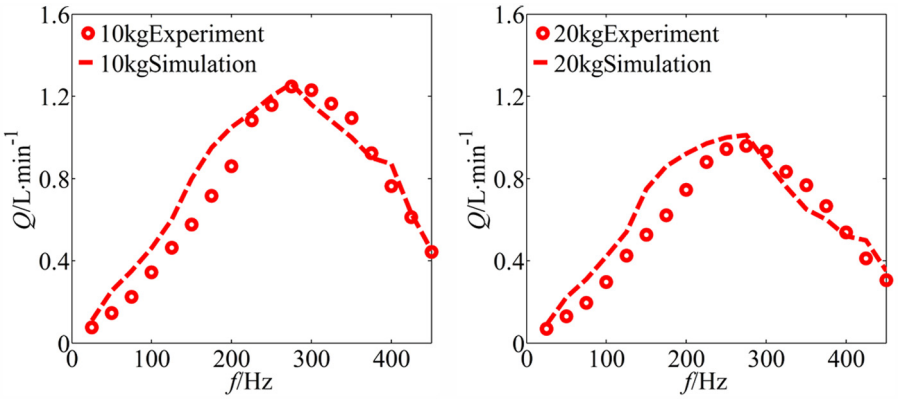

Figure 13. PEHA load performance under fixed weight.

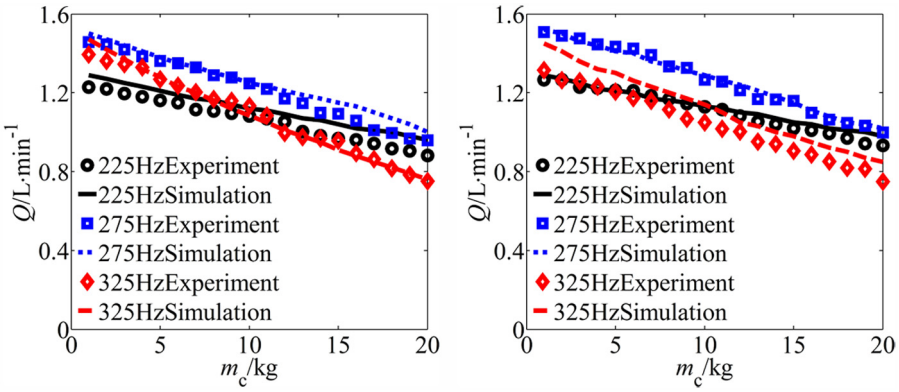

Figure 14. PEHA load performance under increasing weight.

275 Hz. The load capacity is apparently more than 20 kg at certain frequencies.

2. The oil compressibility, reed valve response, inertia, and leakage should be considered in the process of prototyping and modeling. Those factors can be major limitations of the PEHA performance.
3. The accumulator plays an important role in the system. It can provide a bias pressure to prevent cavitation, improve the effective bulk modulus of the fluid and compensate for fluid leakage.
4. The PSA dynamic model was established based on the asymmetric Bouc–Wen model. The model can predict the trend of the PSA output displacement well within 400 Hz.
5. A PEHA time-domain model which consists of the electrical–mechanical, mechanical–hydraulic transformation was established in MATLAB/Simulink. A PSA model, a pump chamber pressure model, a reed valve model, and a fluid model in the tube and hydraulic cylinder were established. The experimental results and simulation results agree with each other well, which demonstrates the feasibility of the model.

Declaration of conflicting interests

The author(s) declared no potential conflicts of interest with respect to the research, authorship, and/or publication of this article.

Funding

The author(s) disclosed receipt of the following financial support for the research, authorship, and/or publication of this article: This work was supported by the National Natural Science Foundation of China (grant number 51575258), Qing Lan Project, SAST Foundation (2016081), and Foundation of Graduate Innovation Center in NUAA (grant number kfjj20170521).

References

Chaudhuri A (2008) *Self-contained hybrid electro-hydraulic actuators using magnetostrictive and electrostrictive materials*. PhD Thesis, University of Maryland, College Park, MD.

Chaudhuri A and Wereley NM (2010) Experimental validation of a hybrid electrostrictive hydraulic actuator analysis. *Journal of Vibration and Acoustics* 132(2): 021006.

Chaudhuri A and Wereley NM (2012) Compact hybrid electrohydraulic actuators using smart materials: a review. *Journal of Intelligent Material Systems and Structures* 23(6): 597–634.

Chaudhuri A, Yoo JH and Wereley NM (2009) Design, test and model of a hybrid magnetostrictive hydraulic actuator. *Smart Materials and Structures* 18(8): 085019.

Chopra I and Sirohi J (2013) *Smart Structures Theory*. Cambridge: Cambridge University Press.

Dong R and Tan Y (2009) A modified Prandtl–Ishlinskii modeling method for hysteresis. *Physica B: Condensed Matter* 404(8): 1336–1342.

Hegewald T, Kaltenbacher B, Kaltenbacher M, et al. (2008) Efficient modeling of ferroelectric behavior for the analysis of piezoceramic actuators. *Journal of Intelligent Material Systems and Structures* 19(10): 1117–1129.

Ismail M, Ikhouane F and Rodellar J (2009) The hysteresis Bouc-Wen model: a survey. *Archives of Computational Methods in Engineering* 16(2): 161–188.

John S, Chaudhuri A and Wereley NM (2008) A magnetorheological actuation system: test and model. *Smart Materials and Structures* 17(2): 025023.

Kim GW (2009) *Design and nonlinear force control of a power-by-wire piezoelectric-hydraulic pump actuator for automotive transmissions*. PhD Thesis, The Pennsylvania State University, State College, PA.

Kim GW and Wang KW (2009a) On-line estimation of effective bulk modulus in fluid power systems using piezoelectric transducer impedance. *Journal of Intelligent Material Systems and Structures* 20(17): 2101–2106.

Kim GW and Wang KW (2009b) Switching sliding mode force tracking control of piezoelectric-hydraulic pump-based friction element actuation systems for automotive transmissions. *Smart Materials and Structures* 18(8): 085004.

Kim GW and Wang KW (2010a) Enhanced control performance of a piezoelectric-hydraulic pump actuator for automotive transmission shift control. *Proceedings of the Institution of Mechanical Engineers, Part D: Journal of Automobile Engineering* 224(2): 161–174.

Kim GW and Wang KW (2010b) Helmholtz resonance in a piezoelectric–hydraulic pump-based hybrid actuator. *Smart Materials and Structures* 20(1): 015010.

Konishi K (1999) Hydraulic actuators driven by piezoelectric elements. *Journal of Japan Society of Mechanical Engineers* 30(7): 512–516.

Li J, Fu YL and Wang ZL (2004) System design and simulation of a new aircraft electro-hydrostatic actuator. *Journal of System Simulation* 16(6): 1128–1131.

Li W, Chen X and Li Z (2013) Inverse compensation for hysteresis in piezoelectric actuator using an asymmetric rate-dependent model. *Review of Scientific Instruments* 84(11): 115003.

Low TS and Guo W (1995) Modeling of a three-layer piezoelectric bimorph beam with hysteresis. *Journal of Microelectromechanical Systems* 4(4): 230–237.

Mauck LD and Lynch CS (2000) Piezoelectric hydraulic pump development. *Journal of Intelligent Material Systems and Structures* 11(10): 758–764.

Sanders B, Crowe R and Garcia E (2004) Defense advanced research projects agency-smart materials and structures demonstration program overview. *Journal of Intelligent Material Systems and Structures* 15(4): 227–233.

Sha NS and Li J (2004) Research on airborne power-by-wire integrated electrical actuation and control systems. *Journal of Beijing University of Aeronautics and Astronautics* 30(9): 909–1024.

Sirohi J and Chopra I (2002) Design and development of a high pumping frequency piezoelectric-hydraulic hybrid actuator. *Journal of Intelligent Material Systems and Structures* 14(3): 135–147.

Song J and Kiureghian AD (2006) Generalized Bouc–Wen model for highly asymmetric hysteresis. *Journal of Engineering Mechanics* 132(6): 610–618.

Sreeram PN and Naganathan NG (1994) Hysteresis prediction for piezoceramic actuator systems using Preisach models. *Proceedings of the Society of Photo-optical Instrumentation Engineers (SPIE)* 2189: 14–25.

Tan HH, Hurst W and Leo D (2010) Performance modeling of a piezohydraulic actuation system with active valves. *Smart Materials and Structures* 14(1): 91–110.

Tang P, Palazzolo A, Kascak A, et al. (1995) Combined piezoelectric-hydraulic actuator based active vibration control for rotordynamic system. *Journal of Vibration and Acoustics* 117(3): 285–293.

Tao BQ (1997) *Intelligent Material Structure*. Leeds: National Defend Industry Press.

Ullmann A and Fono I (2002) The piezoelectric valve-less pump-improved dynamic model. *Journal of Microelectromechanical Systems* 11(6): 655–664.

Walters TE (2008) *Development of a smart material electrohydrostatic actuator considering rectification valve dynamics and in situ valve characterization*. PhD Thesis, The Ohio State University, Columbus, OH.

Wang G, Chen G and Bai F (2015) Modeling and identification of asymmetric Bouc–Wen hysteresis for piezoelectric actuator via a novel differential evolution algorithm. *Sensors and Actuators A: Physical* 235: 105–118.

Zhu W and Rui XT (2016) Hysteresis modeling and displacement control of piezoelectric actuators with the frequency-dependent behavior using a generalized Bouc–Wen model. *Precision Engineering: Journal of the International Societies for Precision Engineering and Nanotechnology* 43: 299–307.

Zhu W and Wang D (2012) Non-symmetrical Bouc–Wen model for piezoelectric ceramic actuators. *Sensors and Actuators A: Physical* 181: 51–60.

Zhu YC and Ji L (2014) Theoretical and experimental investigations of the temperature and thermal deformation of a giant magnetostrictive actuator. *Sensors and Actuators A: Physical* 218: 167–178.

Zhu YC and Li YS (2014) Development of a deflector-jet electrohydraulic servovalve using a giant magnetostrictive material. *Smart Materials and Structures* 23: 115001.

Zhu YC and Li YS (2015) A hysteresis nonlinear model of giant magnetostrictive transducer. *Journal of Intelligent Material Systems and Structures* 26(16): 2242–2255.

Zhu YC, Yang XL and Wereley NM (2016) Research on hysteresis loop considering the prestress effect and electrical input dynamics for a giant magnetostrictive actuator. *Smart Materials and Structures* 25(8): 085030.